Journal of Applied Fluid Mechanics, Vol. 15, No. 6, pp. 1771-1787, 2022.
Available online at www.jafmonline.net, ISSN 1735-3572, EISSN 1735-3645.
https://doi.org/10.47176/jafm.15.06.33536

On Accuracy of Lattice Boltzmann Method Coupled with Cahn-Hilliard and Allen-Cahn Equations for Simulation of Multiphase Flows at High-Density Ratios

E. Ezzatneshan† and A. A. Khosroabadi

Faculty of New Technologies and Aerospace Engineering, Shahid Beheshti University, Tehran, Iran

†*Corresponding Author Email: e_ezzatneshan@sbu.ac.ir*

(Received November 7, 2021; accepted June 16, 2022)

ABSTRACT

In this work, the accuracy of the multiphase lattice Boltzmann method (LBM) based on the phase-field models, namely the Cahn-Hilliard (C-H) and Allen-Cahn (A-C) equations, are evaluated for simulation of two-phase flow systems with high-density ratios. The mathematical formulation and the schemes used for discretization of the derivatives in the C-H LBM and A-C LBM are presented in a similar notation that makes it easy to implement and compare these two phase-field models. The capability and performance of the C-H LBM and A-C LBM are investigated, specifically at the interface region between the phases, for simulation of flow problems in the two-dimensional (2D) and three-dimensional (3D) frameworks. Herein, the equilibrium state of a droplet and the practical two-phase flow problem of the rising bubble are considered to evaluate the mass conservation capability of the phase-filed models employed at different flow conditions and the obtained results are compared with available numerical and experimental data. The effect of employing different equations proposed in the literature for calculating the relaxation time on the accuracy of the implemented phase-field LBMs in the interfacial region is also studied. The present study shows that the LBM based on the A-C equation (A-C LBM) is advantageous over that based on the C-H equation in dealing with the conservation of the total mass of a two-phase flow system. Also, the results obtained by the A-C LBM is more accurate than those obtained using the C-H LBM in comparison with other numerical results and experimental observations. The present study suggests the A-C LBM as a sufficiently accurate and computationally efficient phase-field model for the simulation of practical two-phase flows to resolve their structures and properties even at high-density ratios.

Keywords: Lattice Boltzmann method; Multiphase flows; Cahn-Hilliard equation; Allen-Cahn equation; Comparative study.

NOMENCLATURE

C	fluid concentration
c_s	speed of sound
E_0	bulk energy
$\boldsymbol{e}$	particle velocity
F	force
$\boldsymbol{G}$	gravitational acceleration
g	momentum distribution function
h	concentration distribution function
i	component index
$\boldsymbol{j}$	volume diffusive
M	mobility
P	pressure
R	radius
t	time
$\boldsymbol{u}$	local velocity
$\boldsymbol{x}$	position
α	lattice direction index
β	constant parameter
Γ	hydrodynamic equilibrium function
κ	coefficient related to surface tension
μ	chemical potential
ν	kinematic viscosity
ζ	interface thickness
ρ	density
σ	surface tension
τ	relaxation time
ϕ	order parameter
ω	weighting coefficient

1. INTRODUCTION

Due to the mesoscopic nature of the interfacial interaction, the lattice Boltzmann method (LBM) is a powerful alternative and well-established numerical method for studying multiphase flow problems (Holdych, Rovas *et al*. 2011, Ezzatneshan and Vaseghnia 2020). Despite significant advances in the LBM, resolving the interface region between the phases is still a challenging task in the interfacial flows with high-density ratios (HDR) (Fakhari, Mitchell *et al*. 2017). There are several works to improve the numerical stability and performance of the LBM for the numerical solution of HDR multiphase flows (Inamuro, Ogata *et al*. 2004, Lee and Lin 2005, Bao and Schaefer 2013, Hejranfar and Ezzatneshan 2015, Wang, Shu *et al*. 2015, Zhao, Zhang *et al*. 2019). One of the most appropriate LBM approaches for HDR flow simulations are diffuse-interface models developed based on the phase-field theory (Zu and He 2013). In these models, two-phase flow properties vary continuously across the interface with a smooth transition that provides a great advantage for the study of complex interfacial dynamics in HDR multiphase flows (Liang, Xu *et al*. 2018).

The phase-field methods proposed for the LBM can be categorized as the models developed based on the Cahn-Hilliard (C-H) equation (Cahn and Hilliard 1958) and those of proposed based on the Allen-Cahen (A-C) equation (Allen and Cahn 1976). The LBM based on the C-H equation (C-H LBM) is a diffuse-interface capturing technique that is developed by minimizing a free-energy functional. The chemical potential calculation in the C-H LBM allows evaluating the interfacial dynamics by considering the curvature effects. Accordingly, the difference in the chemical potential of the fluids in this method creates a force imbalance to lead the multiphase system to the equilibrium state to minimize the free energy of the system. However, the LBM based on the A-C equation (A-C LBM) is an interface tracking method that uses a collision invariant to define the phase indicator. In this phase-filed approach, the balance between the fluxes of advection, diffusion, and phase separation across the interface evolves the multiphase system (Su, Li *et al*. 2018, Otomo, Zhang *et al*. 2019, Yan, Ye *et al*. 2021).

In the past decade, simulation of multiphase flows have been performed by the phase-field models based on the C-H and A-C equations (Wang, Yuan *et al*. 2019). Based on the C-H LBM, Lee and Lin (Lee and Lin 2005) and Lee and Liu (Lee and Liu 2010) have developed numerical techniques with two distribution functions, one for computing the pressure and velocity fields and the other calculates an index parameter for the interface capturing. They have employed hybrid finite-difference (FD) schemes for evaluating the forcing terms so that stable numerical solutions are obtained for simulation of HDR multiphase flows. Employing FD schemes for spatial discretization of the gradients in the Lee *et al*.'s approach is not suitable for the local solution of the LBM and reduces the efficiency of the method in parallel computations. Although several attempts have been made to develop an entirely local C-H LBM (Spencer, Halliday *et al*. 2011, Tölke, Prisco *et al*. 2013), the FD discretization techniques are implemented in most of the studies in this area for computing the spatial derivatives until now (Lou and Guo 2015, Lee 2019). Based on the A-C LBM, Sun and Beckermann (Sun and Beckermann 2007) have proposed a phase-field model, which is later reshaped into a conservative form by Chiu and Lin (Chiu and Lin 2011). By using central moments in the formulation of the A-C LBM, Geier *et al*. (Geier, Fakhari *et al*. 2015) have extended this approach to be purely local in the collision step and sufficiently accurate for the interface tracking even in 3D multiphase flow problems. An LBM approach based on the A-C equation is also proposed by Ren *et al*. (Ren, Song *et al*. 2016) that is employed for the simulation of two-phase flows limited up to moderate density ratios. Fakhari *et al*. (Fakhari, Geier *et al*. 2016) have improved the efficiency of the A-C LBM by extension its capabilities for implementation on non-uniform grids. The improved A-C LBM by Fakhari *et al*. is then employed successfully for the simulation of several applied multiphase flows (Fakhari, Bolster *et al*. 2017, Fakhari, Li *et al*. 2018).

Regarding the literature review addressed above, although the C-H LBM and A-C LBM represent similar behaviors in the category of the phase-field methods, some key differences between these two models are notified that affect their accuracy and performance for simulation of multiphase flows, particularly at HDR flow conditions. In the mathematical formulation, the C-H LBM employs second and fourth-order spatial derivatives that compromise the locality of the solutions and reduce the numerical accuracy due to the need for calculating of duplicated Laplacian terms (Fakhari, Geier *et al*. 2019). On the other hand, the A-C LBM only uses first-order and second-order spatial derivatives for tracking the interfacial dynamics that is simple and efficient for parallel computation and dealing with complex boundaries. Another important difference addressed in the literature for C-H LBM and A-C LBM is their capability to conserve the mass of a multiphase system (Chiu and Lin 2011, Liang, Shi *et al*. 2014).

Understanding the effect of the using different LBM techniques on the accuracy and performance of the fluid flow simulations is important to choose an appropriate approach according to its substantial capability (Yang and Boek 2013, Ezzatneshan 2018). Such an evaluation for the aforementioned phase-field methods, namely the C-H LBM and A-C LBM, needs to be taken into account when conducting the simulation results obtained by employing these schemes from the physical point of view. In the literature, Wang *et al*.'s work (Wang, Chai *et al*. 2016) is the only comparative study to evaluate the mentioned phase-field models. They have presented a thorough comparison on the order of accuracy and numerical error of the LBM based on the C-H and A-C equations by applying these models for the simulation of some benchmark two-phase flows, e.g.

the problem of Zalesak's disk rotation. Since studying practical multiphase flows is one of the comprehensive capabilities of the phase-field LB models, the assessment of the C-H and A-C equations for such flow problems is considered in the present paper that will be useful for future developments of these methodologies. Although Wang *et al*. (Wang, Yuan *et al*. 2019) recently summarized some two-phase flow applications from the literature which C-H LBM and A-C LBM are applied for simulations reported in those papers, but no comparative study is presented on the capability and accuracy of the two models in their work.

In this work, the treatment of the C-H LBM and A-C LBM is investigated specifically at the interface region between the phases. Moreover, the mathematical formulation of the C-H LBM and A-C LBM is presented with a clear and understandable expression in a similar notation that makes it easy to implement and compare these two models. The accuracy and computational efficiency of these two phase-field LB models are investigated for studying multiphase flow problems at HDR conditions in the two-dimensional (2D) and three-dimensional (3D) frameworks. A stationary droplet is considered to evaluate the mass conservation capability of these models at different flow conditions. The effect of employing different equations proposed in the literature for calculating the relaxation time on the accuracy of the implemented phase-field LBMs in the interfacial region is also studied. Then, the implemented C-H LBM and A-C LBM are applied for prediction of the practical two-phase flow characteristics of the rising bubble, and the obtained results are compared with available numerical and experimental data.

The paper is organized as follows: Section 2 provides a brief introduction to the formulation of the C-H and A-C LBMs. Section 3 presents the results obtained for the comparative study of these numerical approaches. In Section 4, some conclusions are made.

2. MATHEMATICAL FORMULATION

The continuity equation for a two-component multiphase flow system can be expressed as

$$\frac{\partial \tilde{\rho}_i}{\partial t}+\nabla.\tilde{\rho}_i \boldsymbol{u}_i =0 \ , \quad i=1,2 \tag{1}$$

where $\tilde{\rho}_i$ is the local density and $\boldsymbol{u}_i$ indicates the local velocity. These local properties can be computed based on the bulk density ρ_i and the average velocity $\boldsymbol{u}$ as

$$\rho_i \boldsymbol{j}_i = \tilde{\rho}_i(\boldsymbol{u}_i-\boldsymbol{u}) \ , \quad i=1,2 \tag{2}$$

In this equation, $\boldsymbol{j}_i$ defines the volume diffusive flow rate of i^{th} component, where $\boldsymbol{j}_1=-\boldsymbol{j}_2=\boldsymbol{j}$ (Ding, Spelt *et al*. 2007). The interface position $\boldsymbol{x}$ of a multiphase system at time t can be captured by the composition parameter $C=\frac{\tilde{\rho}_1}{\rho_1}$ which satisfies the following equation (Lee 2009)

$$\frac{\partial C}{\partial t}+\nabla.(\boldsymbol{u}C)=-\nabla.\boldsymbol{j} \tag{3}$$

Accordingly, the local averaged density is computed by $\rho=C\rho_1+(1-C)\rho_2$.

In the following, the governing equations of two phase-field LBMs with the C-H (Lee and Liu 2010) and A-C (Geier, Fakhari *et al*. 2015) equations are provided which recover the above-mentioned formulations. Herein, a simple and computationally efficient collision operator based on the single-relaxation-time or so-called Bhatnagar-Gross-Krook (BGK) approximation is considered for the LBM. Calculating schemes of the phase-field gradients for determining the interface region between the phases by the C-H and A-C approaches are presented and compared to each other.

2.1 Governing Equations of C-H LBM

The convective C-H equation can be given according to Eq. (3) by assuming that the diffusive flow rate is proportional to the gradient of the chemical potential μ as

$$\boldsymbol{j}=-M\nabla\mu \tag{4}$$

where M is the mobility. In the present study, M is set to be a positive constant parameter. The chemical potential in the C-H equation is determined by minimizing the free energy and reads

$$\mu=\mu_0-\kappa\nabla^2 C \tag{5}$$

where κ is a coefficient related to the surface tension. The parameter μ_0 is the derivative of the bulk energy $E_0\approx\beta C^2(C-1)^2$ concerning the composition parameter C

$$\mu_0=\frac{\partial E_0}{\partial C} \tag{6}$$

For a planar interface, the profile of C can be stated at the equilibrium state as

$$C(z)=\frac{1+\tanh(\frac{2z}{\zeta})}{2} \tag{7}$$

In the above equations, β is a constant and ζ is the interface thickness which are chosen based on the accuracy and stability of the numerical solutions. For given values of β and ζ, the coefficient κ and surface tension σ can be computed as

$$\kappa=\frac{\beta\zeta^2}{8} \tag{8}$$

$$\sigma=\frac{\sqrt{2\kappa\beta}}{6} \tag{9}$$

The C-H equation given in Eqs. (3) and (4) can be given in the LBM frameworks as follows to recover the concentration C :

$$\frac{\partial h_\alpha}{\partial t}+\boldsymbol{e}_\alpha.\nabla h_\alpha=-\frac{1}{\tau_\phi}(h_\alpha-h_\alpha^{eq})+(\boldsymbol{e}_\alpha-\boldsymbol{u}).\\ [\nabla C-\frac{C}{\rho c_s^2}(\nabla p_1+C\nabla\mu)]\Gamma_\alpha+\nabla.(M\nabla\mu)\Gamma_\alpha \tag{10}$$

where h_α defines the distribution function, $\boldsymbol{e}_\alpha$, τ_ϕ, and $c_s=1/\sqrt{3}$ are the particle velocity, the relaxation time, and the speed of sound, respectively (Fakhari, Mitchell *et al*. 2017). The equilibrium distribution function h_α^{eq} is computed by

$$h_\alpha^{eq}=\omega_\alpha C\left[1+\frac{\boldsymbol{e}_\alpha\boldsymbol{u}}{c_s^2}+\frac{(\boldsymbol{e}_\alpha\boldsymbol{u})^2}{2c_s^4}-\frac{(\boldsymbol{u}\boldsymbol{u})}{2c_s^2}\right] \tag{11}$$

where ω_α is a weighting factor along direction α. Herein, the D2Q9 and D3Q19 models of the LBM are used to discretize the particle velocity for 2D and 3D flow problems, respectively. Schematics of the particle velocity directions for the D2Q9 and D3Q19 LBMs are shown in Fig. 1. Consequently, $\boldsymbol{e}_\alpha$ and ω_α can be given, e.g. in D3Q19 form, as

$$\boldsymbol{e}_\alpha=\begin{cases}(0,0,0) & \alpha=0\\ (\pm1,0,0),(0,\pm1,0),(0,0,\pm1) & \alpha=1-6\\ (\pm1,\pm1,0),(\pm1,0,\pm1),(0,\pm1,\pm1) & \alpha=7-18\end{cases}\\ \omega_\alpha=\begin{cases}\frac{1}{3} & \alpha=0\\ \frac{1}{18} & \alpha=1-6\\ \frac{1}{36} & \alpha=7-18\end{cases} \tag{12}$$

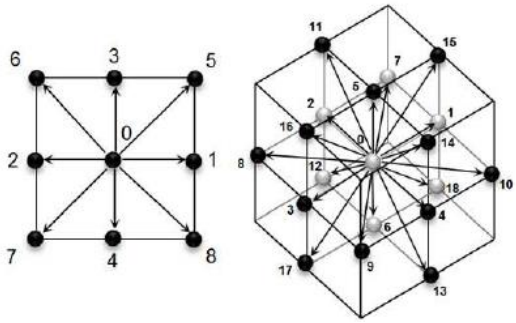

Fig. 1. D2Q9 (left) and D3Q19 (right) lattice models for discretization of particle velocity.

In Eq. (10), p_1 is the hydrodynamic pressure used to enforce incompressibility and Γ_α can be expressed as

$$\Gamma_\alpha=\omega_\alpha\left[1+\frac{\boldsymbol{e}_\alpha\boldsymbol{u}}{c_s^2}+\frac{(\boldsymbol{e}_\alpha\boldsymbol{u})^2}{2c_s^4}-\frac{(\boldsymbol{u}\boldsymbol{u})}{2c_s^2}\right] \tag{13}$$

A new distribution function g_α is employed to recover the pressure and velocity components based on the C-H LBM that reads

$$\frac{\partial g_\alpha}{\partial t}+\boldsymbol{e}_\alpha.\nabla g_\alpha=-\frac{1}{\tau_\phi}(g_\alpha-g_\alpha^{eq})+(\boldsymbol{e}_\alpha-\boldsymbol{u}).\\ [\nabla\rho c_s^2(\Gamma_\alpha-\Gamma_\alpha(0))-(C\nabla\mu+\rho\boldsymbol{G}\nabla h)\Gamma_\alpha]+\\ \boldsymbol{e}_\alpha.(\rho_H\boldsymbol{G}\nabla h)\Gamma_\alpha(0) \tag{14}$$

where $\boldsymbol{G}$ is the gravitational acceleration. The total density is defined by the following linear relation

$$\rho=\rho_H C+\rho_L(1-C) \tag{15}$$

where ρ_H and ρ_L define the density of heavy and light fluids, respectively. The new equilibrium distribution function g_α^{eq} is given by

$$g_\alpha^{eq}=\omega_\alpha\left[P+\rho c_s^2(\frac{\boldsymbol{e}_\alpha\boldsymbol{u}}{c_s^2}+\frac{(\boldsymbol{e}_\alpha\boldsymbol{u})^2}{2c_s^4}-\frac{(\boldsymbol{u}\boldsymbol{u})}{2c_s^2})\right] \tag{16}$$

in which $P=p_1+\rho_H Gh$. The dimensionless relaxation time τ for the multiphase systems studied in the present paper is defined based on the concentration C by the linear and inverse functions. The effect of these functions on the numerical stability and accuracy of the solutions is investigated. According to a linear function, τ is computed as

$$\tau=\tau_H C+\tau_L(1-C) \tag{17}$$

and by taking an inverse function, τ is defined by

$$\frac{1}{\tau}=\frac{C}{\tau_H}+\frac{(1-C)}{\tau_L} \tag{18}$$

It should be noted that the relaxation time τ_i for each fluid is related to the kinematic viscosity ν_i of that fluid by

$$\nu_i=c_s^2\tau_i\delta t\ ,\ i=H,L \tag{19}$$

The C-H LBM given in Eqs. (10) and (14) are discretized along with characteristics over the time step δt in the following forms

$$\bar{h}_\alpha(\boldsymbol{x}+\boldsymbol{e}_\alpha\delta t,t+\delta t)-\bar{h}_\alpha(\boldsymbol{x},\mathrm{t})=\\ -\frac{1}{\tau+0.5}(\bar{h}_\alpha-\bar{h}_\alpha^{eq})\Big|_{(x,t)}+\delta t(\boldsymbol{e}_\alpha-\boldsymbol{u}).\\ [\nabla^{MD}C-\frac{C}{\rho c_s^2}(\nabla^{MD}p_1+C\nabla^{MD}\mu)]\\ \Gamma_\alpha+\ \delta tM(\nabla^2\mu)\Gamma_\alpha\Big|_{(x,t)}\\ \bar{h}_\alpha^{eq}=h_\alpha^{eq}-\frac{\delta t}{2}(\boldsymbol{e}_\alpha-\boldsymbol{u}).\\ [\nabla^{CD}C-\frac{C}{\rho c_s^2}(\nabla^{CD}p_1+C\nabla^{CD}\mu)]\\ \Gamma_\alpha-\frac{\delta t}{2}M(\nabla^2\mu)\Gamma_\alpha] \tag{20}$$

$$\begin{aligned}&\bar{g}_\alpha(\boldsymbol{x}+\boldsymbol{e}_\alpha\delta t,t+\delta t)-\bar{g}_\alpha(\boldsymbol{x},\mathrm{t})=\\&-\frac{1}{\tau+0.5}(\bar{g}_\alpha-\bar{g}_\alpha^{eq})\big|_{(\boldsymbol{x},t)}+\delta t(\boldsymbol{e}_\alpha-\boldsymbol{u}).\\&[\nabla^{MD}\rho c_s^2(\Gamma_\alpha-\Gamma_\alpha(0))-\\&(C\nabla^{MD}\mu+\rho\boldsymbol{G}\nabla h)\Gamma_\alpha]_{(x,t)}+\\&\delta t\boldsymbol{e}_\alpha.(\rho_H\boldsymbol{G}\nabla h)\Gamma(0)_\alpha\big|_{(\boldsymbol{x},t)}\\&\bar{g}_\alpha^{eq}=g_\alpha^{eq}-\frac{\delta t}{2}(\boldsymbol{e}_\alpha-\boldsymbol{u}).\\&[\nabla^{CD}\rho c_s^2(\Gamma_\alpha-\Gamma_\alpha(0))-C\nabla^{CD}\mu\Gamma_\alpha]\end{aligned}\tag{21}$$

In Eqs. (20) and (21), the directional first derivatives of a macroscopic property Q are discretized using the second-order central difference (CD) and mixed difference (MD) schemes (Lee and Lin 2005) as

$$\delta t\,\boldsymbol{e}_\alpha.\nabla^{CD}Q\big|_{(\boldsymbol{x})}=\frac{1}{2}[Q(\boldsymbol{x}+\boldsymbol{e}_\alpha\delta t)-Q(\boldsymbol{x}-\boldsymbol{e}_\alpha\delta t)]\tag{22}$$

$$\delta t\,\boldsymbol{e}_\alpha.\nabla^{MD}Q\big|_{(\boldsymbol{x})}=\frac{1}{2}[\delta t\,\boldsymbol{e}_\alpha.\nabla^{BD}Q+\delta t\,\boldsymbol{e}_\alpha.\nabla^{CD}Q]_{(\boldsymbol{x})}\tag{23}$$

where superscript BD defines the second-order biased difference, e.g. the forward one is

$$\begin{aligned}&\delta t\,\boldsymbol{e}_\alpha.\nabla^{BD}Q\big|_{(\boldsymbol{x})}=\\&\frac{1}{2}[-Q(\boldsymbol{x}+2\boldsymbol{e}_\alpha\delta\mathrm{t})+4Q(\boldsymbol{x}+\boldsymbol{e}_\alpha\delta\mathrm{t})-3Q(\boldsymbol{x})]\end{aligned}\tag{24}$$

The second-order central difference (CD) for the directional second derivatives is also defined by

$$\begin{aligned}&(\delta t\,\boldsymbol{e}_\alpha.\nabla)^2Q\big|_{(\boldsymbol{x})}=\\&[Q(\boldsymbol{x}+\boldsymbol{e}_\alpha\delta t)-2Q(\boldsymbol{x})+Q(\boldsymbol{x}-\boldsymbol{e}_\alpha\delta t)]\end{aligned}\tag{25}$$

Similarly, the differencing schemes for the non-directional first and second derivatives are

$$\nabla^{CD}Q\big|_{(\boldsymbol{x})}=\frac{1}{c_s^2\delta t}\sum_\alpha\omega_\alpha\boldsymbol{e}_\alpha(\delta t\,\boldsymbol{e}_\alpha.\nabla^{CD}Q\big|_{(\boldsymbol{x})})\tag{26}$$

$$\nabla^{MD}Q\big|_{(\boldsymbol{x})}=\frac{1}{2}[\nabla^{BD}Q+\nabla^{CD}Q]_{(\boldsymbol{x})}\tag{27}$$

$$\nabla^{BD}Q\big|_{(\boldsymbol{x})}=\frac{1}{c_s^2\delta t}\sum_\alpha\omega_\alpha\boldsymbol{e}_\alpha(\delta t\,\boldsymbol{e}_\alpha.\nabla^{BD}Q\big|_{(\boldsymbol{x})})\tag{28}$$

$$\nabla^{2}Q\big|_{(\boldsymbol{x})}=\frac{1}{c_s^2\delta t^2}\sum\omega_\alpha(\delta t\,\boldsymbol{e}_\alpha.\nabla)^2Q\big|_{(\boldsymbol{x})}\tag{29}$$

Lou *et al.* (Lou, Guo *et al*. 2012) presented a thorough study on the effect of discretization schemes on the accuracy and stability of two-phase LBM. They have concluded that the mixed-difference scheme can violate the global mass conservation depending on flow conditions and grid resolution. This issue is investigated in the present study for the phase-field LBM based on the C-H equation.

Finally, the composition C, momentum $\rho\boldsymbol{u}$ and the hydrodynamic pressure p_1 can be computed by

$$C=\sum_\alpha\bar{h}_\alpha+\frac{\delta t}{2}M\nabla^2\mu\tag{30}$$

$$\rho\boldsymbol{u}=\frac{1}{c_s^2}\sum_\alpha\boldsymbol{e}_\alpha\bar{g}_\alpha-\frac{\delta t}{2}C\nabla^{CD}\mu\tag{31}$$

$$p_1=\sum_\alpha\bar{g}_\alpha+\frac{\delta t}{2}\boldsymbol{u}.\nabla^{CD}\rho c_s^2\tag{32}$$

2.2 Governing Equations of A-C LBM

To recover the A-C equation as given in Eq. (3), the interface can be tracked by the definition of the order parameter $\phi(\boldsymbol{x},t)$. Then, the volume diffusion flow rate is considered as

$$\boldsymbol{j}=-\nabla.M[\nabla\phi-\frac{\nabla\phi}{|\nabla\phi|}\frac{1-4(\phi-\phi_0)^2}{\xi}]\tag{33}$$

where ξ is the interfacial thickness and $\phi_0=\frac{(\phi_L+\phi_H)}{2}$ defines the position of the interface. Herein, ϕ_L and ϕ_H indicate two extreme values in the bulk of the light and heavy fluids, respectively. For a planar interface, the profile of ϕ at the equilibrium state can be computed by

$$\phi=\phi_0\pm\frac{\phi_H-\phi_L}{2}\tanh(\frac{2(\boldsymbol{x}-\boldsymbol{x}_0)}{\xi})\tag{34}$$

In the present study, Eq. (34) is used to set the initial condition for the phase field. For example, to set a gas bubble suspended in a liquid phase, the minus sign is used, and vice versa. Finally, the interface evolution between two fluids based on the A-C equation is given by

$$\frac{\partial\phi}{\partial t}+\nabla.(\phi\boldsymbol{u})=\nabla.M[\nabla\phi-\frac{\nabla\phi}{|\nabla\phi|}\frac{1-4(\phi-\phi_0)^2}{\xi}]\tag{35}$$

Comparison of the right-hand-side of the C-H and A-C equations given in Eqs. (4) and (33), respectively, shows that the C-H equation includes a fourth-order spatial derivative, while the A-C equation only involves a second-order spatial derivative. Consequently, the discretization and the numerical solution of the A-C equation is more simple and much efficient. It should be noted that if central moments are invoked, the second-order derivative of the A-C equation in the LBM framework can be reduced to the first-order derivative, or even no derivative (Geier, Fakhari *et al*. 2015).

In the LBM framework, the A-C equation defined in Eq. (35) can be discretized as

$$\begin{aligned}&h_\alpha(\boldsymbol{x}+\boldsymbol{e}_\alpha\delta t,t+\delta t)=h_\alpha(\boldsymbol{x},t)-\\&\frac{h_\alpha(\boldsymbol{x},t)-\bar{h}_\alpha^{eq}(\boldsymbol{x},t)}{\tau+0.5}+F_\alpha^\phi(\boldsymbol{x},t)\end{aligned}\tag{36}$$

to recover the order parameter ϕ. In this equation, $\bar{h}_\alpha^{eq}$ is the equilibrium distribution function and F_α^ϕ is the forcing term that are computed by

$$F_\alpha^\phi(\boldsymbol{x},t)=\partial t\frac{[1-4(\phi-\phi_0)^2]}{\xi}\omega_\alpha \boldsymbol{e}_\alpha.\frac{\nabla\phi}{|\nabla\phi|} \tag{37}$$

$$\bar{h}_\alpha^{eq}=h_\alpha^{eq}-0.5F_\alpha^\phi \tag{38}$$

in which $h_\alpha^{eq}=\phi\Gamma_\alpha$ and Γ_α is defined by Eq. (13). Similar to the C-H LBM, the distribution function g_α is employed in the A-C LBM to compute the pressure and velocity components that reads

$$g_\alpha(\boldsymbol{x}+\boldsymbol{e}_\alpha\delta t,t+\delta t)=g_\alpha(\boldsymbol{x},t)-\frac{g_\alpha(\boldsymbol{x},t)-\bar{g}_\alpha^{eq}(\boldsymbol{x},t)}{\tau+0.5}+F_\alpha(\boldsymbol{x},t) \tag{39}$$

The modified equilibrium distribution function $\bar{g}_\alpha^{eq}$ and the hydrodynamic forcing term F_α are computed by

$$\bar{g}_\alpha^{eq}=g_\alpha^{eq}-0.5F_\alpha \tag{40}$$

$$F_\alpha=\delta t\frac{\omega_\alpha \boldsymbol{e}_\alpha.\boldsymbol{F}}{\rho c_s^2} \tag{41}$$

where $g_\alpha^{eq}=p^*\omega_\alpha+(\Gamma_\alpha-\omega_\alpha)$. The parameter $p^*=\frac{p}{\rho c_s^2}$ indicates the normalized pressure and $\boldsymbol{F}$ is the force vector that is defined by

$$\boldsymbol{F}=\boldsymbol{F}_s+\boldsymbol{F}_b+\boldsymbol{F}_p+\boldsymbol{F}_\mu \tag{42}$$

where $\boldsymbol{F}_s$, $\boldsymbol{F}_b$, $\boldsymbol{F}_p$, and $\boldsymbol{F}_\mu$ are the surface tension, body, pressure, and viscous forces, respectively. The mentioned forces are computed by the following relations:

$$\boldsymbol{F}_s=\mu_\phi\nabla\phi \tag{43}$$

$$\boldsymbol{F}_b=-\rho\boldsymbol{G} \tag{44}$$

$$\boldsymbol{F}_p=-p^*c_s^2\nabla\rho \tag{45}$$

$$\boldsymbol{F}_\mu=\nu[\nabla\boldsymbol{u}+(\nabla\boldsymbol{u})^T].\nabla\rho \tag{46}$$

In the above equations, the chemical potential μ_ϕ and the density ρ are expressed as

$$\mu_\phi=4\beta(\phi-\phi_L)(\phi-\phi_H)(\phi-\phi_0)-\kappa\nabla^2\phi \tag{47}$$

$$\rho=\rho_L+(\phi-\phi_L)(\rho_H-\rho_L) \tag{48}$$

As defined in the previous section, the coefficients β and κ can be computed by Eqs. (8) and (9). For the A-C LBM, the linear and inverse functions of τ based on the order parameter ϕ are as follows

$$\tau=\tau_L+(\phi-\phi_L)(\tau_H-\tau_L) \tag{49}$$

$$\frac{1}{\tau}=\frac{1}{\tau_L}+(\phi-\phi_L)(\frac{1}{\tau_H}-\frac{1}{\tau_L}) \tag{50}$$

whwre the kinematic viscosity ν in Eq. (46) is $\nu=c_s^2\tau\delta t$. For the accurate computing of τ in the A-C LBM, Fakhari *et al.* (Fakhari, Mitchell *et al.* 2017) have proposed to use such a linear interpolation for the dynamic viscosity as

$$\mu=\mu_L+(\phi-\phi_L)(\mu_H-\mu_L) \tag{51}$$

and then, τ can be given as

$$\tau=\frac{\mu}{\rho c_s^2\delta t} \tag{52}$$

As mentioned, the major difference between the A-C LBM and the C-H LBM is the schemes used for the discretization of the derivatives in the governing equations. The gradient and Laplacian operators for a macroscopic property Q in the A-C LBM are computed by

$$\nabla Q=\frac{c}{c_s^2\delta\boldsymbol{x}}\sum_\alpha \boldsymbol{e}_\alpha\omega_\alpha Q(\boldsymbol{x}+\boldsymbol{e}_\alpha\delta t,t) \tag{53}$$

$$\nabla^2 Q=\frac{2c^2}{c_s^2(\delta\boldsymbol{x})^2}\sum_\alpha\omega_\alpha[Q(\boldsymbol{x}+\boldsymbol{e}_\alpha\delta t,t)-Q(\boldsymbol{x},t)] \tag{54}$$

As a great advantage for the A-C LBM, these schemes are simple and computationally efficient for calculating the derivatives instead of employing the complicated discretization procedures for the directional and non-directional derivatives implemented in the C-H LBM (see Eqs. (22)-(29)).

Finally, macroscopic parameters ϕ, p^*, and $\boldsymbol{u}$ can be obtained by

$$\phi=\sum_\alpha h_\alpha \tag{55}$$

$$p^*=\sum_\alpha g_\alpha \tag{56}$$

$$\boldsymbol{u}=\sum_\alpha g_\alpha\boldsymbol{e}_\alpha+\frac{\boldsymbol{F}}{2\rho}\delta t \tag{57}$$

The velocity in the A-C LBM is updated after the pressure. Therefore, there is no need for the predictor-corrector scheme which imposes an extra computational cost. Additionally, the density gradient $\nabla\rho$ and the viscous force F_μ in the direction i can be computed from (Fakhari, Mitchell *et al.* 2017)

$$\nabla\rho=(\rho_H-\rho_L)\nabla\phi \tag{58}$$

$$F_{\mu,i}=-\frac{\nu}{(\tau+0.5)c_s^2\delta t}[\sum_\alpha e_{\alpha i}e_{\alpha j}(g_\alpha-g_\alpha^{eq})]\frac{\partial\rho}{\partial x_j} \quad i,j\in(x,y,z) \tag{59}$$

Applying these relations makes ϕ the only non-local variable to compute the density gradient and viscous force that enhances the efficiency of the A-C LBM in comparison with the C-H LBM.

3. RESULTS AND DISCUSSIONS

In this section, the capability of C-H and A-C LBMs presented in the previous section are evaluated for the simulation of different multiphase flows. At first, the numerical results of these models are verified by simulation of the equilibrium state of a droplet suspended in a gas phase that is a well-known benchmark two-phase flow problem. Then, the accuracy and efficiency of the C-H LBM and A-C LBM are compared by the simulation of 2D and 3D two-phase flow systems, including bubble and droplet dynamics. The obtained results are compared with the existing data in the literature in various flow conditions. It should be noted that the density ratio and viscosity ratio are indicated by $\rho^* = \frac{\rho_H}{\rho_L}$ and $\mu^* = \frac{\mu_H}{\mu_L}$, respectively, where $\rho_H = 1$ and $\mu_H = 0.0033$ are set in the present work. Also, the interface thickness ζ is considered to be 5, and the constant parameter $M \times \beta$ is set to be 3×10^{-4} in all the simulations unless otherwise specified.

3.1 Model Validation

For a 2D liquid droplet suspended in the gas phase, the surface tension σ causes a pressure difference Δp between the outside and inside of the droplet. The Laplace law (Weil 1984) defines a linear relation between σ and Δp for a certain droplet radius R as

$$\Delta p = p_{in} - p_{out} = \frac{\sigma}{R} \tag{60}$$

The Laplace law is verified by using the present C-H LBM and A-C LBM for the simulation of a stationary droplet placed in a fully periodic square domain with the grid size of 201×201. The solutions are performed for various droplet radiuses at $\rho^* = 100$, $\mu^* = 20$, and $\sigma = 10^{-5}$. Herein, the droplet with the radiuses $R = 25$, $R = 35$, and $R = 45$ is initialized in the center of the flowfield. The initial phase field is also defined by Eqs. (7) and (34) for the C-H LBM and A-C LBM, respectively, to preserve the stability of the numerical solutions at the beginning iterations (Ezzatneshan 2017). Figure 2 illustrates the results obtained for Δp versus $1/R$ by using the C-H LBM and A-C LBM after the droplet reaches to the equilibrium state. For the present solutions, it takes about 5×10^5 time steps for the liquid-gas system established to reach the equilibrium state using both the phase-field models employed. The linear relation between Δp and $1/R$ in Fig. 2 shows that the present C-H and A-C LBMs satisfy the Laplace law. Linear fits are in good agreement, except for the well-known offset from the origin (Lycett-Brown and Luo 2015). The value of the surface tension is computed by the slope of each line that is obtained $\sigma = 1.1\times10^{-5}$ and 1.0×10^{-5} by the C-H LBM and A-C LBM, respectively. As seen in Fig. 2, the slope of the fitted line on the simulation results of the stationary droplet by employing the A-C LBM is 1.0×10^{-5} that shows an excellent match with the $\sigma = 10^{-5}$ set in the simulation. However, there is a slight difference between the value obtained for the surface tension based on the slope of the fitted line on the C-H LBM results with that set in the algorithm. This difference can be depending on the accuracy of this model which has been affected by the mass conservation property and its capability in the capturing interface. Such characteristics of the C-H LBM and A-C LBM are discussed in detail in Sec. 3.2.

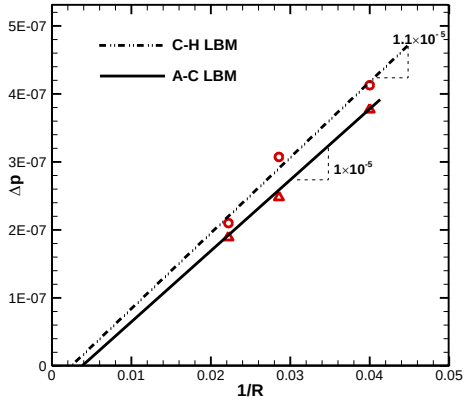

Fig. 2. Verification of Laplace law for a stationary droplet suspended in gas phase by employing C-H LBM and A-C LBM.

In the multiphase LBMs, the existence of the undesirable spurious velocity in the interfacial region is due to the interaction forces and imbalance between stresses in the liquid-gas interface. These parasitic currents can be reduced by the implementation an appropriate discretization technique for computing the forcing terms (Mattila, Siebert *et al*. 2013). Herein, the maximum magnitude of the spurious velocity $\left|u^s_{max}\right|$ and the corresponding Capillary number $Ca = \mu\left|u^s_{max}\right|/\sigma$ are given in Table 1 for the simulation results obtained for the droplet suspended in the gas phase at different radiuses using the C-H LBM and A-C LBM. Although the results show that both the models produce negligible spurious velocity, the magnitude of $\left|u^s_{max}\right|$ computed by employing the A-C LBM is higher than that of obtained based on the C-H LBM. In the following discussions, it is shown that the A-C LBM resolves the interface region with a slightly sharper profile than the C-H LBM that can be the main reason for a bit higher spurious velocities in the interface for the A-C LBM.

Table 1. Comparison of $|u^s_{max}|$ and Ca obtained for a stationary droplet suspended in gas phase by employing C-H LBM and A-C LBM.

R		C-H LBM	A-C LBM
25	$\|u^s_{max}\|$	3.49×10^{-9}	5.58×10^{-8}
	Ca	1.2×10^{-6}	1.9×10^{-5}
35	$\|u^s_{max}\|$	1.19×10^{-8}	4.37×10^{-8}
	Ca	4.0×10^{-6}	1.5×10^{-5}
45	$\|u^s_{max}\|$	3.36×10^{-8}	3.65×10^{-8}
	Ca	1.1×10^{-5}	1.2×10^{-5}

3.1 Comparison Study in Two-dimensional Framework

At first, the mass conservation property of the implemented phase-field models is checked by simulation of the stationary droplet to examine the efficiency of the C-H LBM and A-C LBM in the 2D framework. This two-phase flow problem is studied in a periodic square domain with 101×101 lattice nodes in which a droplet with $R=20$, $\rho^*=1000$, $\mu^*=100$, and $\sigma=10^{-5}$ is placed in the center of the flow domain. In Fig. 3, the shape of the droplet at the initial time is compared with that obtained at the equilibrium state after $t=5\times10^5$ iterations by the C-H LBM and A-C LBM. The droplet modeled using the C-H LBM shrinks due to losing mass, while the shape of the droplet simulated by employing the A-C LBM does not significantly change during the solution.

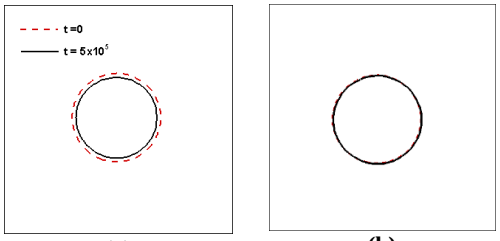

(a) **(b)**

Fig. 3. Mass conservation study for a stationary 2D droplet with $\rho^*=1000$ and $\mu^*=100$ by employing (a) C-H LBM, and (b) A-C LBM.

To have a quantitative comparison on the mass conservation property of these two phase-field models for simulation of the 2D stationary droplet, the variation of the total mass of the two-phase system is plotted in Fig. 4. This figure shows that the A-C LBM preserves the total mass, while for the C-H LBM the mass of the two-phase system decreases at the beginning iterations and then, gradually increases. This study shows that although the results obtained for the 2D stationary droplet by the C-H LBM satisfy with the Laplace law, this model is not mass conservative. The effect of this undesirable feature on the flow parameters in the system is examined by investigation of the density and velocity profiles through the domain.

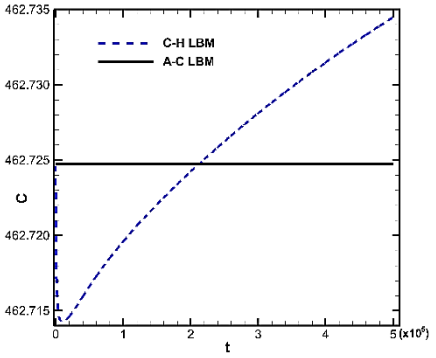

Fig. 4. Comparison of total mass variation obtained for a stationary 2D droplet with $\rho^*=1000$ and $\mu^*=100$ by employing C-H LBM and A-C LBM.

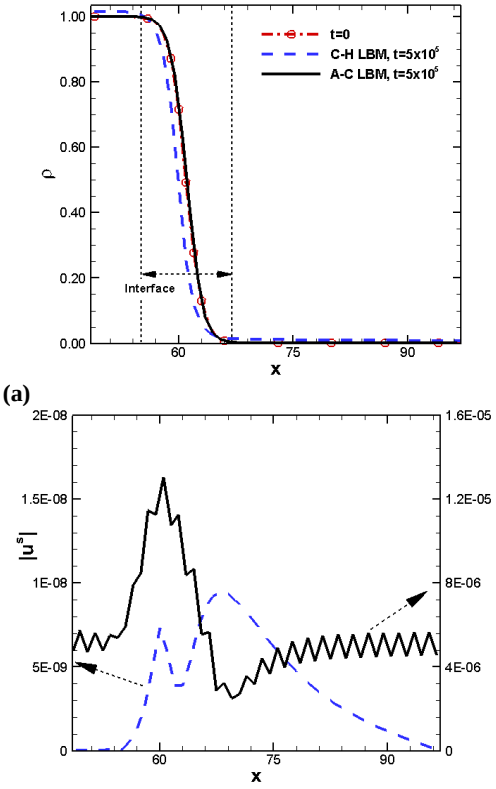

Fig. 5. Comparison of density (a) and velocity (b) profiles obtained for a stationary 2D droplet with $\rho^*=1000$ and $\mu^*=100$ by employing C-H LBM and A-C LBM.

The comparison of the density and velocity profiles obtained based on the C-H LBM and A-C LBM for the equilibrium state of the stationary droplet with $R=20$, $\rho^*=1000$, $\mu^*=100$, and $\sigma=10^{-5}$ is shown in Fig. 5. These profiles are plotted at the mid-line of the 2D domain, from the center of the droplet to the right boundary. As observed in this figure, the density profile predicted using the A-C LBM at the equilibrium state is quite consistent with that provided as the initial condition which confirms the

mass conservation property of this model. The value of liquid and gas densities obtained based on the C-H LBM, however, significantly affected by the loss of the mass and does not match with the density ratio set at the initial condition. Note that the A-C LBM provides a slightly sharper interface in the density profile compared with the C-H LBM. Although it is expected zero velocity magnitude at the equilibrium state of the stationary droplet, the velocity profile presented in Fig. 5 indicates the existence of spurious velocities $|u^s|$ in the simulation results for the 2D equilibrated liquid-gas system based on both the phase-field models employed. By using the A-C LBM, the maximum value of $|u^s|$ in the interface region is higher than that calculated by the implementation of the C-H LBM. The sharpness of the interface profile in the A-C LBM can be the main reason for the higher values of the spurious velocity. On the other hand, loss of the mass in the C-H LBM causes a smooth profile in the interface region and consequently produces weak spurious currents.

The accuracy of the implemented phase-field models is also compared to determine how the simulation results of these multiphase LBMs depend on the calculation of the relaxation time τ at the interface region. Figure 6 compares the profiles of τ computed based on the linear and inverse functions across a planar interface with $\tau_H = 0.01$ and $\tau_L = 0.1$. This figure illustrates that the variation of relaxation time for both the functions is monotonic with respect to the position at the interface of the liquid-gas system.

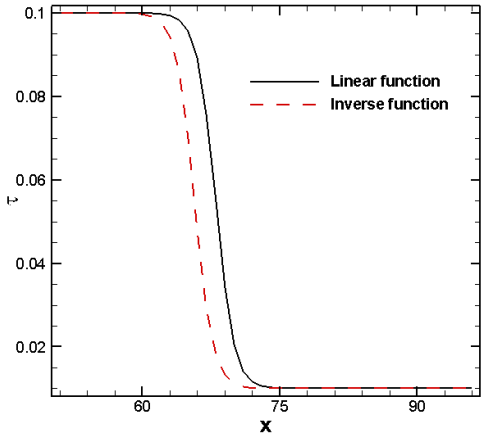

Fig. 6. Comparison of τ profiles computed by linear and inverse functions in interface region.

The effect of these relaxation time distribution across the interface is examined on the density and velocity profiles obtained by the C-H LBM and A-C LBM in Figs. 7 and 8, respectively. This comparison study is performed for the stationary droplet with $\mu^* = 100$ at two density ratios $\rho^* = 10$ and $\rho^* = 1000$. Generally, it can be seen that the function used for calculation of τ has no significant effect on the distribution of the density in the liquid-gas flowfield simulated by using C-H LBM and A-C LBM. However, the spurious velocities in the interface region are affected by τ profiles which show the method of the relaxation time calculation can impact

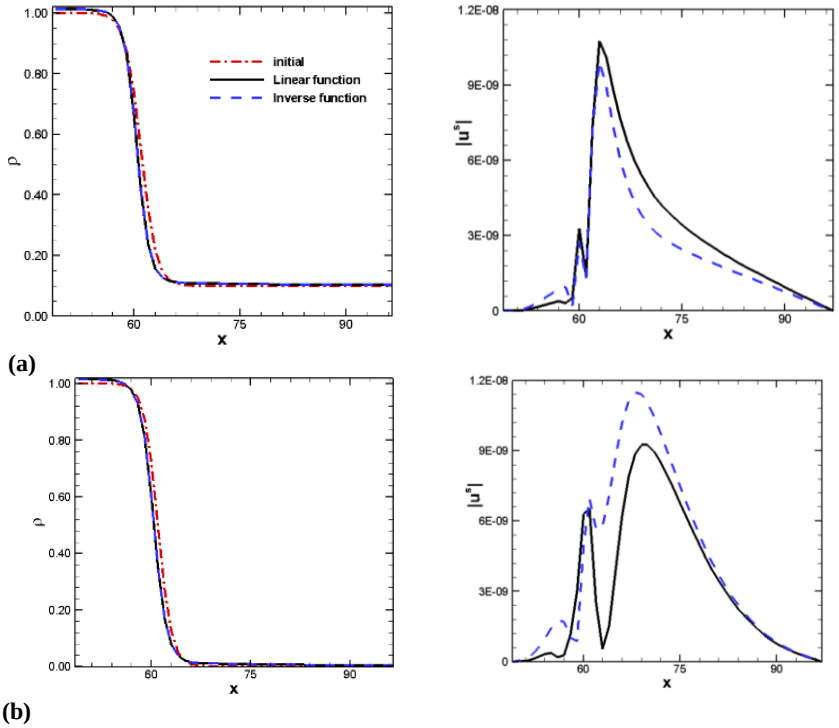

Fig. 7. Comparison of density (left) and velocity (right) profiles obtained for a stationary 2D droplet with $\mu^* = 100$, and $\rho^* = 10$ (a) and $\rho^* = 1000$ (b) by employing C-H LBM.

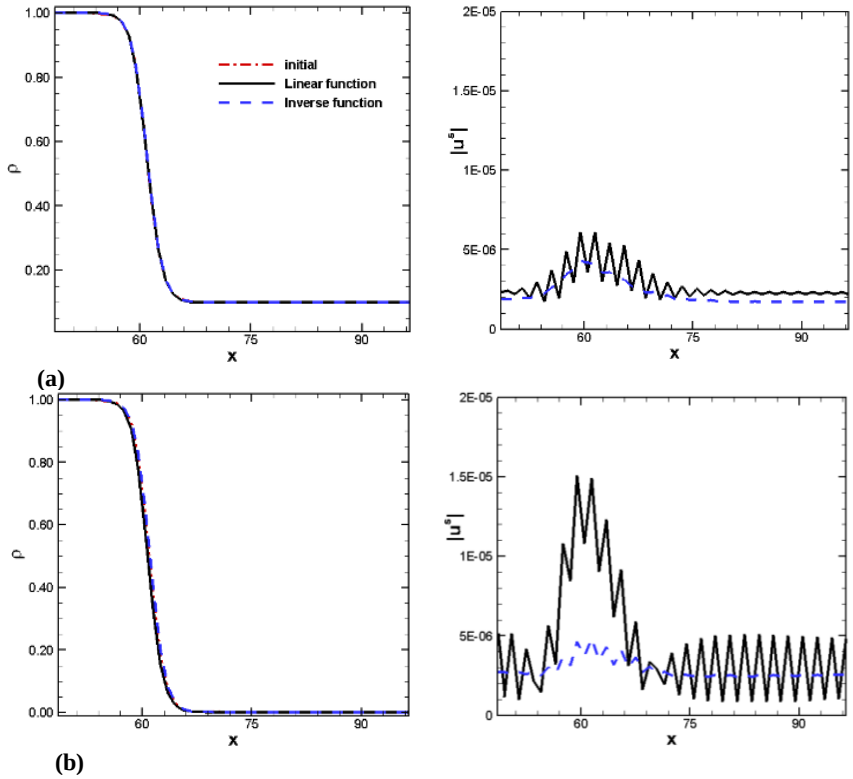

Fig. 8. Comparison of density (left) and velocity (right) profiles obtained for a stationary 2D droplet with $\mu^* = 100$, and $\rho^* = 10$ (a) and $\rho^* = 1000$ (b) by employing A-C LBM.

the numerical stability of the solutions. For the lower density ratio $\rho^* = 10$, this impact is not considerable in both the models. While at the high-density ratio $\rho^* = 1000$, the magnitude of the spurious velocity calculated at the interface region based on the inverse function of τ is higher than that obtained by linear function for the simulations by the C-H LBM. For the A-C LBM, the linear function produced stronger spurious currents at the interface region of the stationary droplet with $\rho^* = 1000$. From Figs. 7 and 8, it also can be seen that the mass conservation property of the phase-field models employed in the present study does not depend on the relaxation time distribution. The droplet shrinks by using the C-H LBM with both the relaxation time functions at the density ratios considered, while the A-C LBM preserves the total mass to be conserved in the flowfield at all the conditions studied.

A comparison study is performed on the capability of the C-H LBM and A-C LBM for the simulation of the stationary droplet at high-density ratio and the obtained results are presented in Fig. 9. The highest value of the density ratio that is possible to resolve by these models with a numerically stable solution is defined. The present study shows that the C-H LBM is stable for the density ratio up to order of 10^4. However, the A-C LBM preserves the stability of the solution for the density ratio up to order of 10^6. The efficiency of the applied C-H and A-C LBMs is investigated by the comparison of the computational cost. The run time measured for the simulation of the stationary 2D droplet is given in Table 2. This

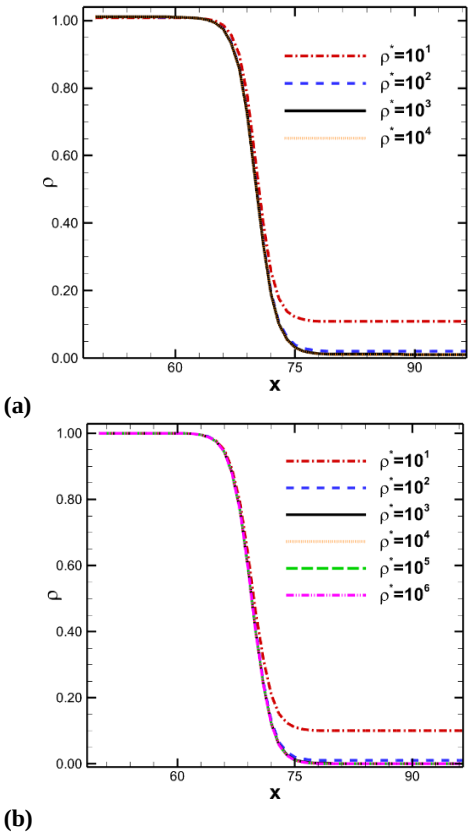

Fig. 9. Comparison of density profiles obtained for a stationary 2D droplet with $\mu^* = 100$ at different density ratios by employing (a) C-H LBM and (b) A-C LBM.

comparison shows that the A-C LBM has about 20% less computational cost for the solution of this test case to reach the time of $t = 5\times10^5$. The differencing scheme used to discretize the derivatives in the C-H equation can be the main reason for its higher computational cost.

Table 2. Comparison of computational cost for simulation of a stationary 2D droplet with C-H LBM and A-C LBM for $t = 5\times10^5$ time steps.

Method	Run time (minutes)
C-H LBM	12.6
A-C LBM	10.5

The capability and efficiency of the C-H LBM and A-C LBM for predicting characteristics of practical liquid-gas flows are investigated by simulation of a rising bubble under the influence of buoyancy force in the 2D framework. In this study, an unconfined domain is considered with 240×960 grid size, and two effective non-dimensional numbers, namely Bond number $Bo = \frac{G_y \Delta\rho (2R)^2}{\sigma}$ and Morton number $Mo = \frac{G_y \Delta\rho \mu_H^4}{\sigma^3 \rho_H^2}$, are defined. In these definitions, G_y is the gravity in y direction and $\Delta\rho = \rho_H - \rho_L$.

Figure 10 illustrates the comparison between the results for the rising bubble obtained based on the C-H LBM and A-C LBM at two flow conditions with $Bo = 1000$ and $Mo = 48000$, and $Bo = 240$ and $Mo = 260$. It is obvious that the loss of the mass in the solution results of the C-H LBM impacts the shape of the bubble and its dynamics during the rising process. The area of the bubble shape computed based on the C-H LBM simulations is decreased during the solution. While the area of the rising bubble modeled by employing the A-C LBM is preserved constantly due to the mass conservation property of this model. However, if such a comparison is not made, the appearance of the bubble resulting from the present numerical solutions based on both the C-H LBM and A-C LBM in Fig. 10 seems comparable with those expected according to the shape regime map (R. Clift 1978) at the given Bo and Mo numbers. This comparison shows the importance of the present study in determining the advantages and shortcomings of the numerical methods applied. Accordingly, it can be concluded that the phase-field LBM based on the A-C equation is more accurate than the C-H LBM for the simulation of two-phase flow systems in the 2D framework.

3.1 Comparison Study in Three-dimensional Framework

The comparison study between the phase-field LBMs implemented based on the C-H and A-C equations is performed in a 3D framework to examine their accuracy and efficiency for simulation of practical multiphase flows. The equilibrium state

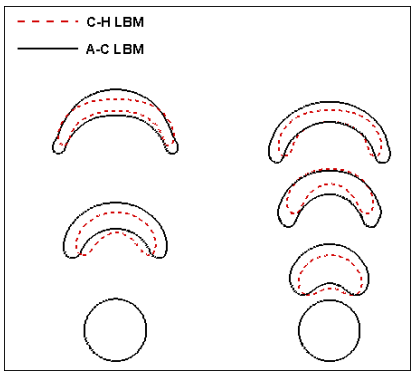

Fig. 10. Comparison of results obtained for a rising 2D bubble at $Bo = 1000$ and $Mo = 48000$ (left), and $Bo = 240$ and $Mo = 260$ (right) by employing C-H LBM and A-C LBM.

of a 3D stationary droplet in a periodic cubic domain with $101\times101\times101$ is considered to investigate the mass conservation property of the C-H LBM and A-C LBM. In this study, the droplet radius is set to be $R = 20$, and the properties of the two-phase system are $\mu^* = 100$ and $\sigma = 10^{-5}$. Herein, two density ratios $\rho^* = 10$ and 1000 are used to demonstrate the capability of the phase-field models employed in resolving the interface region for the 3D stationary droplet simulations.

In Fig. 11, the shape of the droplet at the initial time is compared with that obtained at the equilibrium state after $t = 2\times10^5$ iterations by the C-H LBM and A-C LBM. The shape of the 3D droplet at the equilibrium condition obtained by applying the C-H LBM shrinks during the simulation due to losing mass, while the A-C LBM provides the equilibrium state of the droplet with similar shape and mass of the system as set at the initial condition. The obtained results also show that the mass conservation property of these phase-field models does not depend on the magnitude of the density ratio.

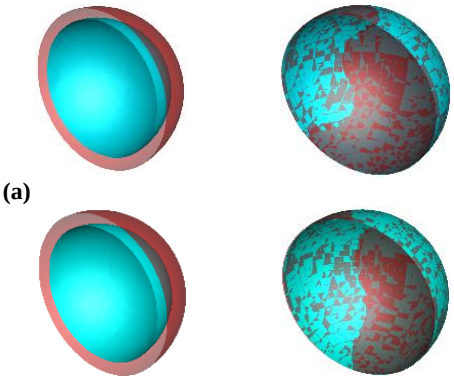

Fig. 11. Mass conservation study for a stationary 3D droplet suspended in gas phase with $\mu^* = 100$, and (a) $\rho^* = 10$ and (b) $\rho^* = 1000$ by employing C-H LBM (left), and A-C LBM (right).

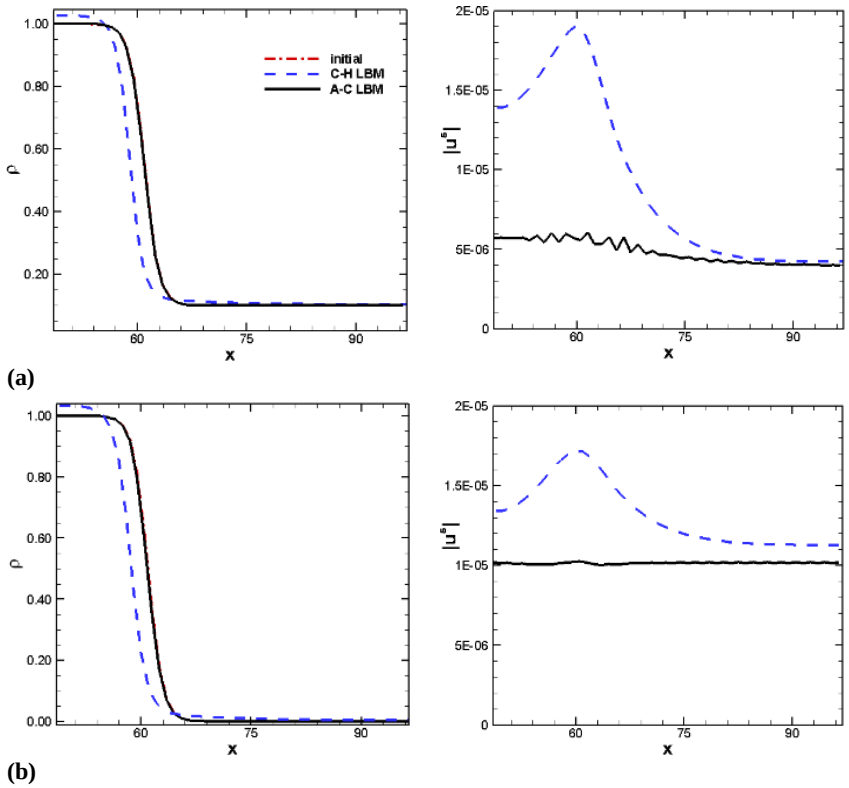

Fig. 12. Comparison of density (left) and velocity (right) profiles obtained for a stationary 3D droplet suspended in gas phase with $\mu^* = 100$, and (a) $\rho^* = 10$ and (b) $\rho^* = 1000$ by employing C-H LBM and A-C LBM.

The effect of the losing and conserving mass by the C-H LBM and A-C LBM, respectively, on the density and velocity fields of the two-phase system includes the 3D stationary droplet is examined in Fig. 12. This figure shows the comparison of the density and velocity profiles obtained based on these models for the equilibrium state of the droplet at the flow conditions considered in Fig. 11. As illustrated in this figure, the density profile predicted using the A-C LBM at the equilibrium state is quite consistent with that provided as the initial condition at both the density ratios $\rho^* = 10$ and 1000, which confirms the mass conservation of this model. However, the density profiles obtained by employing the C-H LBM for the equilibrium state is deviated from the initial profile due to the lack of mass conservation. Similar to the 2D simulations performed for the equilibrium state of the droplet, the results presented in Fig. 12 for the 3D stationary droplet demonstrate the existence of spurious velocities in the interface region. Note that by increasing the density ration from $\rho^* = 10$ to 1000, the magnitude of the spurious velocity obtained based on both the C-H LBM and A-C LBM is increased. The magnitude of the spurious velocity produced in the interfacial region of the 3D droplet by using the A-C LBM is lower than that obtained by the C-H LBM. This comparison study confirms that the A-C LBM is more accurate than the C-H LBM in terms of mass conservation. Although the stability of these two phase-field models can be affected with an increment of the density ratio due to increasing the spurious currents, the A-C LBM can preserve the stability of the numerical solution of two-phase flow systems because of producing weaker spurious currents.

The 3D simulation of bubble rising under the influence of gravitational force is performed to assay the capability of the C-H LBM and A-C LBM for predicting the characteristics of such a practical multiphase flow problem. Herein, the dynamic behavior of a rising bubble is studied in a rectangular cuboid flow domain with $144 \times 144 \times 240$ lattice nodes at different flow conditions and the results obtained are compared with numerical and experimental data. Figure 13 shows the present results obtained for the rising bubble shape based on the C-H LBM and A-C LBM at two flow conditions with $Bo = 1000$ and $Mo = 48000$, and $Bo = 240$ and $Mo = 260$. For more clarity and ease of comparison, a subzone of the domain is presented in this figure that shows half of the flowfield. The difference in the deformation in the interface region between the shape of the bubble predicted by these phase-field models is obvious, particularly at the last snapshot when the bubble reached the terminal velocity (final shape). This study shows that A-C LBM exhibits more deformation than C-H LBM, which can be attributed to the mass conservation in the simulations based on the A-C LBM. On the other hand, the A-C LBM preserves the initial volume of the bubble and therefore, the rising bubble size in the A-C LBM simulations is larger than that in the solutions by C-H LBM that consequents more deformation.

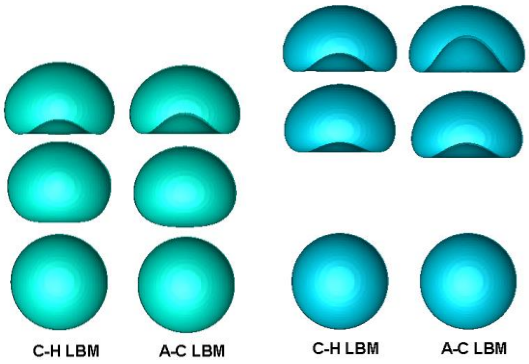

(a) **(b)**

Fig. 13. Comparison of results obtained for a rising 3D bubble at (a) $Bo = 1000$ **and** $Mo = 48000$ **, and (b)** $Bo = 240$ **and** $Mo = 260$ **by employing C-H LBM and A-C LBM.**

To examine the accuracy of the C-H LBM and A-C LBM in predicting the shape of the rising bubble presented in Fig. 13, the current result obtained with both the models for the final shape of the bubble after reaching the terminal velocity is compared with that obtained by an LBM solution (Amaya-Bower and Lee 2010) and an experimental observation (Bhaga and Weber 2006) at flow condition $Bo = 240$ and $Mo = 260$ in Fig. 14. As can be seen in the figure, the rising bubble shape obtained by employing A-C LBM is more comparable with previous computational and experimental data which indicates the better accuracy of this model in comparison with the C-H LBM.

For the quantitative verification of the current results obtained for the rising bubble at $Bo = 240$ and $Mo = 260$, the terminal Reynolds number of the bubble $\mathrm{Re}_t = \frac{\rho_H U_t (2R)}{\mu_H}$, computed according to the terminal velocity U_t, is given in Table 3. This comparison shows that the terminal Reynolds number obtained by the A-C LBM is in excellent agreement with the experimental data that confirms the accuracy and efficiency of this model in comparison with the C-H LBM.

Table 3. Comparison of terminal Reynolds number Re_t **obtained for a rising bubble at** $Bo = 240$ **and** $Mo = 260$**.**

	Method	Re_t
	Experimental (Bhaga and Weber 2006)	7.8
	Numerical (Amaya-Bower and Lee 2010)	6.2
	C-H LBM	6.7
	A-C LBM	7.8

According to the experimental observations (Bhaga and Weber 2006), a relationship between the drag coefficient C_d of a rising bubble and its terminal Reynolds number Re_t is established as

$$C_d = \left[(2.67)^{0.9} + \left(\frac{16}{\mathrm{Re}_t} \right)^{0.9} \right]^{\frac{1}{0.9}} \tag{61}$$

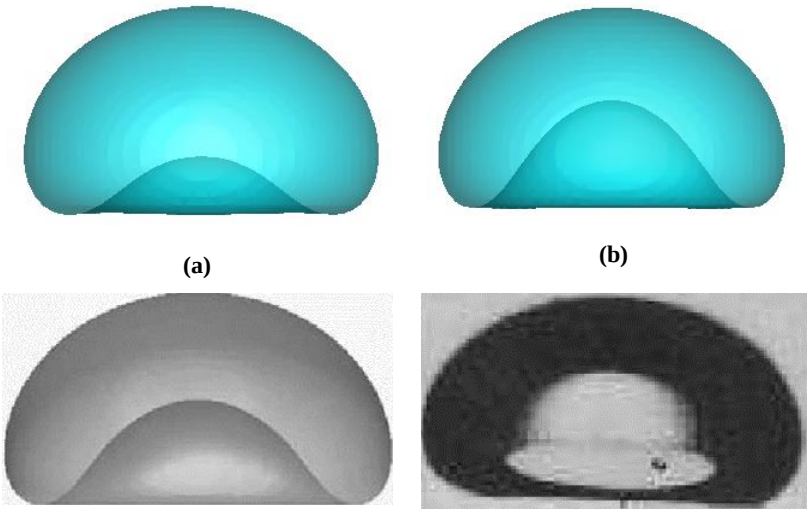

(a) **(b)**

(c) **(d)**

Fig. 14. Results obtained for a rising 3D bubble at $Bo = 240$ **and** $Mo = 260$ **by employing (a) C-H LBM, and (b) A-C LBM, in comparison with (c) numerical result presented in Ref. (Amaya-Bower and Lee 2010), and (d) experimental observation in Ref. (Bhaga and Weber 2006).**

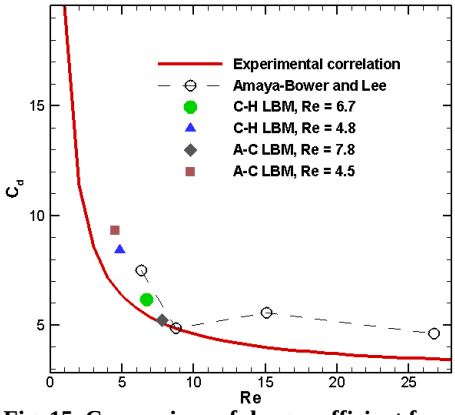

Fig. 15. Comparison of drag coefficient for a rising 3D bubble obtained by employing C-H LBM and A-C LBM with numerical results (Amaya-Bower and Lee 2010) and experimental correlation (Bhaga and Weber 2006) at flow conditions defined in Fig. 13.

Figure 15 shows the comparison between the present results obtained for the C_d of the rising bubble versus its Re_t with that of reported in Refs. (Bhaga and Weber 2006, Amaya-Bower and Lee 2010) at the flow conditions considered in Fig. 13. It can be seen that the present simulation results are in good agreement with the previous computational data, although the predicted C_d versus Re_t based on the present A-C LBM is more consistent with the experimental correlation at higher Reynolds numbers. The relative error between the present numerical results and the experimental correlation is given in Table 4. There is a deviation between the experimental data and the numerical results, particularly at the lower Reynolds number. Similar discrepancy between numerical results and experimental data for the drag coefficient of a rising bubble is also reported in the literature (Fakhari and Rahimian 2010, Amaya-Bower and Lee 2011). Such a discrepancy can be due to the diffuse interface characteristic of numerical methods based on multiphase LBMs which leads to inaccurate predictions at the diffusion dominant flow conditions.

Table 4. Relative error of drag coefficient predicted by present numerical results in comparison with the experimental correlation for a rising bubble at $Bo = 240$ and $Mo = 260$.

Test case	*Error* (%)
C-H LBM, $\mathrm{Re} = 6.7$	12
C-H LBM, $\mathrm{Re} = 4.8$	30
A-C LBM, $\mathrm{Re} = 7.8$	2
A-C LBM, $\mathrm{Re} = 4.5$	36

Finally, the capability of the A-C LBM in resolving more complex interfacial dynamics is demonstrated by the simulation of a rising bubble at two flow conditions with $Bo = 24$ and $Mo = 0.0034$, and $Bo = 240$ and $Mo = 0.0434$. As illustrated in Fig. 16 for $Bo = 24$ and $Mo = 0.0034$, the bottom surface of the bubble is deformed throughout the trajectory until an oblate ellipsoidal cap is formed. With the increment of the effective non-dimensional numbers to $Bo = 240$ and $Mo = 0.0434$, the bubble shape transforms from the spherical cap to a toroidal shape during the rising process that is comparable with that expected according to the shape regime map (R. Clift 1978) and other computational results (Amaya-Bower and Lee 2010). The present study confirms the accuracy and stability of the A-C LBM for simulation of complex practical multiphase flows with preserving the total mass of the system in 3D frameworks.

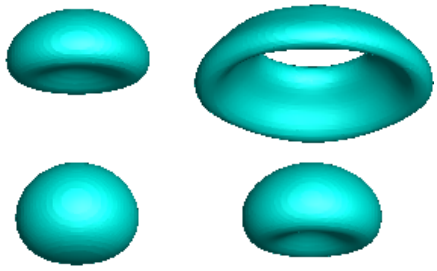

(a) **(b)**

Fig. 16. 3D bubble rising at (a) $Bo = 24$ and $Mo = 0.0034$, and (b) $Bo = 240$ and $Mo = 0.0434$ by employing A-C LBM.

4. CONCLUSION

In this work, the capability and efficiency of the lattice Boltzmann method (LBM) coupled with two phase-field models based on the Cahn-Hilliard (C-H) and Allen-Cahn (A-C) equations are examined for simulation of two-phase flow systems with high-density ratios. The mathematical formulation and the schemes used for discretization of the derivatives in the C-H LBM and A-C LBM are presented and the accuracy and performance of these two models are evaluated for simulation of flow problems in the two-dimensional (2D) and three-dimensional (3D) frameworks. Herein, the equilibrium state of a droplet and also, the practical two-phase flow problem of the rising bubble are considered to investigate the mass conservation property of the phase-filed models employed at different flow conditions and the obtained results are compared with available numerical and experimental data.

It is indicated that the numerical results for the equilibrium state of a 2D stationary droplet obtained based on both the C-H LBM and the A-C LBM satisfy the Laplace law, although the A-C LBM accurately predicts the surface tension of this two-phase flow in comparison with the C-H LBM. The present study shows that the C-H LBM has a serious failure in the total mass conservation of the two-phase systems studied in the 2D and 3D frameworks. The droplet and bubble shapes obtained based on this phase-field model shrink due to loss of the mass that significantly impacts its accuracy for the computation of the flow structure and characteristics. The mixed-differencing scheme used to discretize

the derivatives in the C-H equation is the main reason for the non-mass conservation issue. On the other hand, it is shown that the A-C LBM is an efficient phase-field model in terms of the mass conservation and the results obtained by employing this model are in good agreement with the previous computational simulations and experimental observations. Also, the study of the flow properties, e.g. the density and velocity variations, in the interface region illustrates that the C-H LBM does not preserve the density ratio set for the flow problem during the simulation, while the density profile obtained based on the A-C LBM is exact the same with that of defined in the initial condition. Both the models produce very small spurious currents in the interfacial region which is not considerable in comparison with the flow velocities in the practical two-phase flows studied, e.g. the rising bubble. In conclusion, the present study suggests the A-C LBM by taking into account the mass conservation property, preserving the density ratio, numerical stability at higher density ratios, and also due to the acceptable accuracy for the simulation of practical two-phase flows to resolve their structures and properties even at high-density ratios.

ACKNOWLEDGEMENTS

The authors would like to thank Shahid Beheshti University for the support of this research.

REFERENCES

Allen, S. M. and J. W. Cahn (1976). Mechanisms of phase transformations within the miscibility gap of Fe-rich Fe-Al alloys. *Acta Metallurgica* 24(5), 425-437.

Amaya-Bower, L. and T. Lee (2010). Single bubble rising dynamics for moderate Reynolds number using Lattice Boltzmann Method. *Computers & Fluids* 39(7), 1191-1207.

Amaya-Bower, L. and T. Lee (2011). Numerical simulation of single bubble rising in vertical and inclined square channel using lattice Boltzmann method. *Chemical Engineering Science* 66(5), 935-952.

Bao, J. and L. Schaefer (2013). Lattice Boltzmann equation model for multi-component multi-phase flow with high density ratios. *Applied Mathematical Modelling* 37(4), 1860-1871.

Bhaga, D. and M. E. Weber (2006). Bubbles in viscous liquids: shapes, wakes and velocities. *Journal of Fluid Mechanics* 105, 61-85.

Cahn, J. W. and J. E. Hilliard (1958). Free Energy of a Nonuniform System. I. Interfacial Free Energy. *The Journal of Chemical Physics* 28(2), 258-267.

Chiu, P. H. and Y. T. Lin (2011). A conservative phase field method for solving incompressible two-phase flows. Journal of Computational Physics 230(1), 185-204.

Clift, R., J. R. G., M. E. Weber. (1978). *Bubbles, drops, and particles*. New York ; London, Academic Press.

Ding, H., P. D. M. Spelt and C. Shu (2007). Diffuse interface model for incompressible two-phase flows with large density ratios. *Journal of Computational Physics* 226(2), 2078-2095.

Ezzatneshan, E. (2017). Study of surface wettability effect on cavitation inception by implementation of the lattice Boltzmann method. *Physics of Fluids* 29(11), 113304.

Ezzatneshan, E. (2019). Comparative study of the lattice Boltzmann collision models for simulation of incompressible fluid flows. *Mathematics and Computers in Simulation* 156, 158-177

Ezzatneshan, E. and H. Vaseghnia (2020). Evaluation of equations of state in multiphase lattice Boltzmann method with considering surface wettability effects. *Physica A: Statistical Mechanics and its Applications* 541, 123258.

Fakhari, A., D. Bolster and L. S. Luo (2017). A weighted multiple-relaxation-time lattice Boltzmann method for multiphase flows and its application to partial coalescence cascades. *Journal of Computational Physics* 341, 22-43.

Fakhari, A., M. Geier and D. Bolster (2019). A simple phase-field model for interface tracking in three dimensions. *Computers & Mathematics with Applications* 78(4), 1154-1165.

Fakhari, A., M. Geier and T. Lee (2016). A mass-conserving lattice Boltzmann method with dynamic grid refinement for immiscible two-phase flows. *Journal of Computational Physics* 315, 434-457.

Fakhari, A., Y. Li, D. Bolster and K. T. Christensen (2018). A phase-field lattice Boltzmann model for simulating multiphase flows in porous media: Application and comparison to experiments of CO2 sequestration at pore scale. *Advances in Water Resources* 114, 119-134.

Fakhari, A., T. Mitchell, C. Leonardi and D. Bolster (2017). Improved locality of the phase-field lattice-Boltzmann model for immiscible fluids at high density ratios. *Physical Review E* 96(5-1), 053301.

Fakhari, A. and M. H. Rahimian (2010). Phase-field modeling by the method of lattice Boltzmann equations. *Physical Review E* 81(3 Pt 2), 036707.

Geier, M., A. Fakhari and T. Lee (2015). Conservative phase-field lattice Boltzmann model for interface tracking equation. *Physical Review E* 91(6), 063309.

Hejranfar, K. and E. Ezzatneshan (2015). Simulation of two-phase liquid-vapor flows using a high-order compact finite-difference lattice Boltzmann method. *Phys Rev E Stat Nonlin Soft Matter Phys* 92(5), 053305.

Holdych, D. J., D. Rovas, J. G. Georgiadis and R. O. Buckius (2011). An Improved Hydrodynamics Formulation for Multiphase Flow Lattice-Boltzmann Models. *International Journal of Modern Physics C* 09(08), 1393-1404.

Inamuro, T., T. Ogata, S. Tajima and N. Konishi (2004). A lattice Boltzmann method for incompressible two-phase flows with large density differences. Journal of Computational Physics 198(2), 628-644.

Lee, T. (2009). Effects of incompressibility on the elimination of parasitic currents in the lattice Boltzmann equation method for binary fluids. *Computers & Mathematics with Applications* 58(5), 987-994.

Lee, T. (2019). Fully implicit force splitting scheme to two-phase lattice Boltzmann equation in pressure-velocity formulation. *72nd Annual Meeting of the APS Division of Fluid Dynamics* 64(13), November 23–26, Seattle, Washington.

Lee, T. and C. L. Lin (2005). A stable discretization of the lattice Boltzmann equation for simulation of incompressible two-phase flows at high density ratio. *Journal of Computational Physics* 206(1), 16-47.

Lee, T. and L. Liu (2010). Lattice Boltzmann simulations of micron-scale drop impact on dry surfaces. *Journal of Computational Physics* 229(20), 8045-8063.

Liang, H., B. C. Shi, Z. L. Guo and Z. H. Chai (2014). Phase-field-based multiple-relaxation-time lattice Boltzmann model for incompressible multiphase flows. *Physical Review E* 89(5), 053320.

Liang, H., J. Xu, J. Chen, H. Wang, Z. Chai and B. Shi (2018). Phase-field-based lattice Boltzmann modeling of large-density-ratio two-phase flows. *Physical Review E* 97(3), 033309.

Lou, Q. and Z. Guo (2015). Interface-capturing lattice Boltzmann equation model for two-phase flows. *Physical Review E* 91(1), 013302.

Lou, Q., Z. L. Guo and B. C. Shi (2012). Effects of force discretization on mass conservation in lattice Boltzmann equation for two-phase flows. *EPL (Europhysics Letters)* 99(6), 64005.

Lycett-Brown, D. and K. H. Luo (2015). Improved forcing scheme in pseudopotential lattice Boltzmann methods for multiphase flow at arbitrarily high density ratios. *Physical Review E* 91(2), 023305.

Mattila, K. K., D. N. Siebert, L. A. Hegele and P. C. Philippi (2013). High-Order Lattice-Boltzmann Equations and Stencils for Multiphase Models. *International Journal of Modern Physics C* 24(12), 1340006 .

Otomo, H., R. Zhang and H. Chen (2019). Improved phase-field-based lattice Boltzmann models with a filtered collision operator. *International Journal of Modern Physics C* 30(10), 1941009.

Ren, F., B. Song, M. C. Sukop and H. Hu (2016). Improved lattice Boltzmann modeling of binary flow based on the conservative Allen-Cahn equation. *Physical Review E* 94(2-1), 023311.

Spencer, T. J., I. Halliday and C. M. Care (2011). A local lattice Boltzmann method for multiple immiscible fluids and dense suspensions of drops. *Philosophical Transactions A: Mathematical, Physical and Engineering Sciences* 369(1944), 2255-2263.

Su, T., Y. Li, H. Liang and J. Xu (2018). Numerical study of single bubble rising dynamics using the phase field lattice Boltzmann method. *International Journal of Modern Physics C* 29(11), 1850111.

Sun, Y. and C. Beckermann (2007). Sharp interface tracking using the phase-field equation. *Journal of Computational Physics* 220(2), 626-653.

Tölke, J., G. D. Prisco and Y. Mu (2013). A lattice Boltzmann method for immiscible two-phase Stokes flow with a local collision operator. *Computers & Mathematics with Applications* 65(6), 864-881.

Wang, H., X. Yuan, H. Liang, Z. Chai and B. Shi (2019). A brief review of the phase-field-based lattice Boltzmann method for multiphase flows. *Capillarity* 2(3), 33-52.

Wang, H. L., Z. H. Chai, B. C. Shi and H. Liang (2016). Comparative study of the lattice Boltzmann models for Allen-Cahn and Cahn-Hilliard equations. *Physical Review E* 94(3-1): 033304.

Wang, Y., C. Shu, J. Y. Shao, J. Wu and X. D. Niu (2015). A mass-conserved diffuse interface method and its application for incompressible multiphase flows with large density ratio. *Journal of Computational Physics* 290, 336-351.

Weil, K. G. (1984). J. S. Rowlinson and B. Widom: Molecular Theory of Capillarity, Clarendon Press, Oxford 1982. 327 Seiten. Berichte der Bunsengesellschaft für physikalische Chemie 88(6), 586-586.

Yan, X., Y. Ye, J. Chen, X. Wang and R. Du (2021). Improved multiple-relaxation-time lattice Boltzmann model for Allen–Cahn equation. *International Journal of Modern Physics C*, 32(7), 2150086.

Yang, J. and E. S. Boek (2013). A comparison study of multi-component Lattice Boltzmann models for flow in porous media applications. *Computers & Mathematics with Applications* 65(6), 882-890.

Zhao, W., Y. Zhang and B. Xu (2019). An improved pseudopotential multi-relaxation-time lattice Boltzmann model for binary droplet collision with large density ratio. *Fluid Dynamics Research* 51(2), 025510.

Zu, Y. Q. and S. He (2013). Phase-field-based lattice Boltzmann model for incompressible binary fluid systems with density and viscosity contrasts. *Physical Review E* 87(4), 043301.